An Optical Method for Pretilt and Profile Determination in LCOS VAN Displays

Beatriz Cerrolaza, Morten Andreas Geday, Xabier Quintana, and José Manuel Otón

***Abstract*—Pretilt angle and cell thickness are two extremely important parameters in predicting the behavior of vertically aligned negative nematic liquid crystal (LC) displays. The accurate estimation of pretilt angle and cell thickness is not a trivial task when these devices work in reflective mode, as in liquid crystal on silicon (LCOS) vertically aligned nematic (VAN) displays. Usual experimental setups are based on the proportionality between the retardation of the polarization components of the incident light and the product effective birefringence times thickness. However, any attempt to separate the two product variables is cancelled out by symmetry from reflection. This work shows a relatively simple method capable of separating both variables, allowing accurate, independent measurements of pretilt and thickness, as well as other configurations details, such as residual twist. A simulation model based on the properties of actual reflective displays has been developed. An experimental setup specifically designed for measuring LCOS VAN cells has been prepared. Initial comparisons between experimental measurements of intensity and theoretical results showed some discrepancies that could be explained assuming that the LC profile contains a residual twist from the manufacturing process. Including that twist in the model, an excellent agreement between theory and experiment has been achieved. Matching simulations and experimental results yield separate determinations of pretilt angle and thickness, and give good estimates for the residual twist angle.**

***Index Terms*—Liquid crystal on silicon (LCoS), pretilt angle, reflective display, twist angle, vertically aligned nematic (VAN).**

I. Introduction

VERTICALLY aligned nematic (VAN) liquid crystal (LC) displays with negative dielectric anisotropy have become popular in direct-view display applications [1]. These materials working in reflective mode are also one of the most common choices for high-end projection microdisplays in projection devices [2], where VANs are usually driven by an active-matrix silicon backplane [liquid crystal on silicon (LCOS)].

A negative dielectric anisotropy is the main characteristic of VAN materials, which means that LC molecules will be oriented perpendicularly to any applied electric field above threshold. If the induced alignment were strictly vertical, the LC molecular reorientation in an electric field perpendicular to the cell's outer plates would be undetermined since any position within the plane normal to the field would be energetically equivalent. Moreover, the response time could be dramatically worsened because the electric torque is null for pure vertical alignment. These issues are customarily solved by the induction of a certain pretilt angle in the vertical orientation [3], favoring a specific switching plane and speeding up the switching time. Nevertheless, inducing a pretilt has also a drawback: due to the molecules inclination the relaxed state becomes birefringent and the contrast decays drastically as pretilt increases. Therefore, the correct and precise choice of pretilt angle is a trade-off when designing actual LCOS VAN devices. It follows that accurate measurement of pretilt in actual working devices—and their spatial homogeneity across the cell—is extremely important.

With this objective of accurately measuring the pretilt angle, several techniques have been proposed and applied [4]–[7] such as the magnetic null method, the crystal rotation technique, the polarizer rotation method, and the phase retardation measurement method. All of them are accurate and reliable for pretilt angle measurements in transmissive mode.

However, measuring the pretilt angle in reflective VAN cells like LCOS is a more complex task. The problem is that the birefringence measured at normal incidence is proportional both to the effective birefringence and to the cell thickness. Two methods [8]–[12] proposed for measuring pretilt in these conditions suffer from problems in measuring the photodetector dark current and in normalizing the incident light. Accurate measurements, on the other hand, become a difficult task since pretilt must be measured in the absence of perturbations like applied voltage. Optical measurements of normal or oblique light reflected by the LCOS VAN cell between crossed polarizers in the absence of voltage are extremely low—after all, this is equivalent to measuring the dark state transmission of a commercial LCOS VAN, a device characterized, among other features, by a high contrast.

If these two variables—effective birefringence and thickness—could be separated, pretilt could be derived from birefringence. In this work, we describe in detail a procedure capable of separating the thickness and pretilt dependences. The procedure is based on simultaneous acquisitions of normal and oblique incident light beams of a rotating sample [13]. Simultaneous acquisition does not overcome the problem of

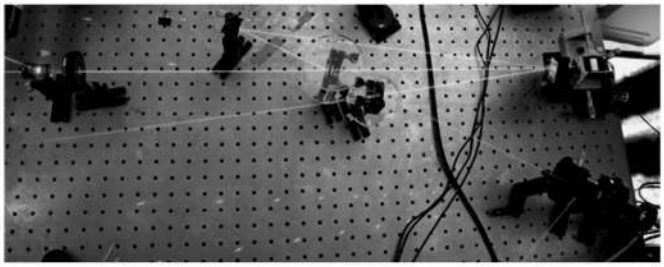

Fig. 1. Experimental setup.

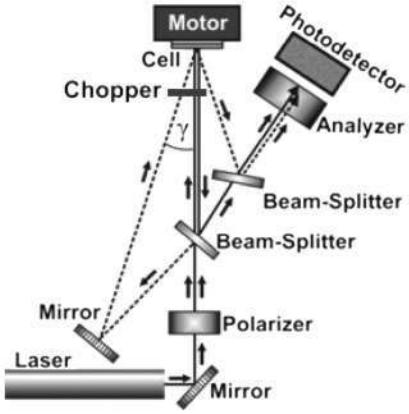

Fig. 2. Sketch of experimental setup shown above. Either normal or oblique beams are alternatively blocked before reaching the photodetector.

low light intensity levels, but provides a procedure to test the validity of fitting parameters by comparing the results of independent acquisitions.

II. Experimental Setup

A picture and a sketch of the experimental setup are shown in Figs. 1 and 2, respectively. A single polarized laser beam is split into two beams after reinforcing the polarization in a Glan-Taylor prism. The LCOS VAN cell is placed in a 5-axis PC-controlled micropositioning system. One of the beams impinges normally to the LCOS VAN surface. The other beam is brought to a mirror for oblique incidence of a controlled angle γ. The $x-y-z-\rho-\theta$ 5-axis system has several functions: 1) to allow the precise positioning of the sample, so that both beams impinge onto the same point; 2) to ease repositioning when incident (zenithal) angle γ is modified; 3) to select different X, Y regions of the sample in order to check the spatial homogeneity of the measurements, and 4) to allow rotation about the azimuthal angle, hence a full set of measurements can be sequentially collected. Both beams are brought to the same photodetector with the same incidence. The light path of either beam is alternatively shuttered by a mechanical chopper, so that only one of the beams reaches the detector at any given time.

III. Mathematical Model

A. Description of the System

The mathematical model is based on the Extended Jones matrix theory [14], and has been developed in Maple 10. The model includes the effects of interfaces and oblique incidence in the impinging beam intensity. Cell is rotating about the point where light impinges on, and the incidence angle may vary from normal incidence to any angle γ from the normal axis.

The coordinate system and angles employed in the model are shown in Fig. 3. All referenced angles $(\beta, \gamma, \theta, \varphi)$ are internal angles, e.g., γ is the angle of the incident light after crossing the glass-LC interface. The cell plates are onto the XY plane and Z-axis is normal to the surface. The pretilt angle β is the angle that is being measured. Rotation of the cell about the Z-axis is defined by φ, while θ is the difference between γ and β. $\overrightarrow{N}$ is the LC director vector, forming an angle β already defined with normal Z. $\overrightarrow{K}$ is the propagation vector of the incident beam forming an angle γ already defined with normal Z.

The starting point for this mathematical model is the definition of a generic refractive index ellipsoid representing the LC molecule

$$\text{ellipsoid} = \begin{bmatrix} n_o \sin\nu \cos u \\ n_o \sin\nu \sin u \\ n_e \cos\nu \end{bmatrix} \tag{1}$$

where ν and u are the ellipsoid parametric latitude and longitude, respectively.

The ellipsoid orientation is determined by the pretilt angle inclination β and the rotation φ about the Z-axis that the cell will experience. $\text{Rot}Z(\varphi)$ is the rotation function about the Z-axis

$$\text{Rot}Z(\varphi) = \begin{bmatrix} \cos\varphi & \sin\varphi & 0 \\ -\sin\varphi & \cos\varphi & 0 \\ 0 & 0 & 1 \end{bmatrix} \tag{2}$$

The inclination due to the pretilt angle is given by $\text{Rot}Y(-\beta)$ function

$$\text{Rot}Y(-\beta) = \begin{bmatrix} \cos\beta & 0 & -\sin\beta \\ 0 & 1 & 0 \\ \sin\beta & 0 & \cos\beta \end{bmatrix} \tag{3}$$

$TR_{\text{ellipsoid}}$ represents the LC molecule with the rotation φ and the inclination β already applied as shown in (4) at the bottom of the page. In order to simplify the mathematical expressions, the coordinate system is rotated. Defining new axes X′, Y′ and

$$TR_{\text{ellipsoid}} = \begin{bmatrix} \cos\varphi\cos\beta \cdot n_o \sin\nu\cos u + \sin\varphi \cdot n_o \sin\nu \sin u - \cos\varphi\sin\beta \cdot n_e \cos\nu \\ -\sin\varphi\cos\beta \cdot n_o \sin\nu\cos u + \cos\varphi \cdot n_o \sin\nu\sin u + \sin\varphi\sin\beta \cdot n_e \cos\nu \\ \sin\beta \cdot n_o \sin\nu\cos u + \cos\beta \cdot n_e \cos\nu \end{bmatrix} \tag{4}$$

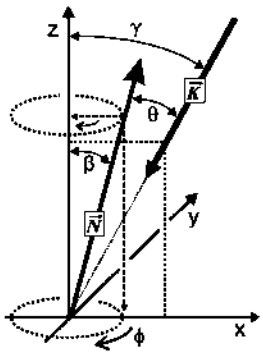

Fig. 3. Coordinate system.

Z′, the oblique incident light is now perpendicular to the new plane X′Y′.

Rot$Y[\gamma]$ induces a rotation equivalent to γ angle previously defined as the angle of the incident beam with the Z-axis of the initial coordinate system

$$\mathrm{Rot}Y(\gamma) = \begin{bmatrix} \cos\gamma & 0 & \sin\gamma \\ 0 & 1 & 0 \\ -\sin\gamma & 0 & \cos\gamma \end{bmatrix} \tag{5}$$

$CRTR_{\mathrm{ellipsoid}}$ is the redefined LC molecular ellipsoid in this new coordinate system.

$$CRTR_{\mathrm{ellipsoid}} = \mathrm{Rot}Y(\gamma) \cdot TR_{\mathrm{ellipsoid}} \tag{6}$$

As defined in the presentation of the coordinate system, $\vec{N}$ is the pretilt director vector, which is a unit vector following the pretilt angle direction

$$\vec{N} = \begin{bmatrix} \sin\beta\cos\varphi \\ \sin\beta\sin\varphi \\ \cos\beta \end{bmatrix}. \tag{7}$$

K is the propagation vector of the impinging beam, which is a unit vector and follows the direction of the incident light after crossing the cell glass plate

$$\vec{K} = \begin{bmatrix} \sin\gamma \\ 0 \\ \cos\gamma \end{bmatrix}. \tag{8}$$

Theta θ is the angle between $\vec{N}$ and $\vec{K}$, obtained as the inverse cosine of the vector product of these two unit vectors

$$\theta = \cos^{-1}[\cos\gamma\cos\beta + \sin\gamma\cos\varphi\sin\beta]. \tag{9}$$

The orthogonal components of the electric field of the impinging light beam, for any given oblique incidence, are parallel to the orientations of the LC ordinary index n_o and to an effective index n_{eff}, generically defined as

$$n_{\mathrm{eff}} = \frac{1}{\sqrt{\dfrac{\cos\xi^2}{n_e^2} + \dfrac{\sin\xi^2}{n_o^2}}} \tag{10}$$

where ξ is the polar angle between incident beam and extraordinary axis.

The effective index expressed in terms of predefined angles looks like (11) at the bottom of the page. From this effective index, effective birefringence (Δn), as "seen" by the incident light, is defined as the difference between n_{eff} and the ordinary index n_o

$$\Delta n = n_{\mathrm{eff}} - n_o \tag{12}$$

The cell is to be rotated about the Z axis. A negative gamma ($-\gamma$) rotation is applied to the molecular director vector $\vec{N}$; this is equivalent to a positive γ rotation about the axis. $\vec{N}'$ is the new director vector in the rotated coordinate system where the incident beam is normal to the X′Y′ plane

$$\vec{N} = \begin{bmatrix} \cos\gamma\sin\beta\cos\varphi - \sin\gamma\cos\beta \\ \sin\beta\sin\varphi \\ \cos\gamma\cos\beta + \sin\gamma\cos\varphi\sin\beta \end{bmatrix}. \tag{13}$$

In the case of a null pretilt ($\beta = 0$), the newly defined director vector depends only on γ

$$\vec{N}'(\beta = 0) = \begin{bmatrix} -\sin\gamma \\ 0 \\ \cos\gamma \end{bmatrix} \tag{14}$$

$tanum$ is defined as the ratio between the y and x components of the new vector $\vec{N}'$, with a minus sign affecting the all expression. Applying the arctangent function to the defined variable $tanum$, the angle α formed by the projection of $\vec{N}'$ on the new X′Y′ plane normal to the impinging light with changed sign is obtained

$$tanum = -\frac{\sin\beta\sin\varphi}{\cos\gamma\sin\beta\cos\varphi - \sin\gamma\cos\beta} \tag{15}$$

$$\alpha = \tan^{-1}(tanum). \tag{16}$$

B. Single Path Intensity Plots

Let us first consider the case of a transmissive cell, where the incident beam only travels once across the LC medium before reaching the detector. The intensity of the impinging beam is defined as $Inten0$

$$Inten0 = \sin(-2\alpha)^2 \sin\left(\frac{\delta}{2}\right)^2 \tag{17}$$

$$n_{\mathrm{eff}} = \sqrt{\frac{1}{\dfrac{1-[\cos\gamma\cos\beta + \sin\gamma\cos\varphi\sin\beta]^2}{n_e^2} + \dfrac{[\cos\gamma\cos\beta + \sin\gamma\cos\varphi\sin\beta]^2}{n_o^2}}}. \tag{11}$$

TABLE I
VALUES USED IN SOME SIMULATIONS WITH 1° PRETILT

$\gamma = 0$	*impinging beam is perpendicular to the XY plane*
$\beta = \pi/180$	*radians corresponding to 1° pretilt angle*
$n_e = 1.65$	*extraordinary refractive index*
$n_o = 1.5$	*ordinary refractive index*
$L = 1.3$	*cell thickness in μm*
$\lambda = 544$	*wavelength in nm*
$bk = 2 \cdot 10^{-6}$	*background intensity of incident light*

where δ is the delay between the electric field components of the light beam:

$$Inten0 = \sin(-2\alpha)^2 \sin\left(\frac{\pi \cdot \Delta n \cdot L}{\lambda}\right)^2 \tag{18}$$

with Δn as the effective birefringence defined in (12) and L as the cell thickness.

Assigning the specific values shown in Table I. to the free variables of $Inten0$, the intensity plot presented in Fig. 4 is obtained by the simulation model.

For normal incidence a classical symmetrical four-leaf clover response is obtained, as shown in Fig. 4. The light intensity is very low, as shown in the figure. Increasing the incidence angle with respect to the normal, two of the petals vanish out and the curve loses its vertical symmetry. The maximum value of the detected intensity increases with the incidence angle, and the four-leaf clover becomes a hunched eight shown in Fig. 5.

C. Double Path Intensity Plots

Let us now consider the double path case, corresponding to reflective displays such as LCOS VANs. With two optical paths the intensity expression derived for two crossed polarizers is not applicable. Instead, two sequential retarders must be considered to simulate the LC action. One corresponds to $\gamma = \gamma_0$ and the other to $\gamma = \gamma_0 + 180°$. Also α and Δn are different in the incident and reflected paths. The delay induced by the double path of the cell depends on birefringence, sample thickness, and wavelength

$$\delta = \frac{2\pi \cdot \Delta n \cdot L}{\lambda}. \tag{19}$$

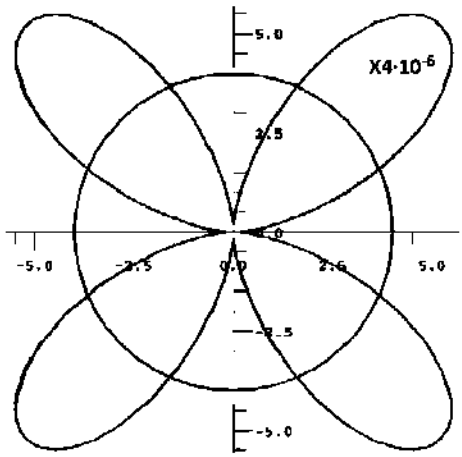

Fig. 4. Polar plot of light intensity in a transmissive cell with 1° pretilt. The circle is a reference value $4 \cdot 10^{-6}$ for every rotating angle φ, showing the extremely low transmission of the cell.

Birefringence for the first path is called Δn_1, and depends on φ_0, that is, the value assigned to the incidence angle γ, shown in (20) at the bottom of the page. Δn_2 is the birefringence for the return path after reflection on the mirror surface. In this case, $\gamma = \gamma_0 + 180$ as shown in (21) at the bottom of the page.

The corresponding expression for the defined variable α (16) in the case of the incident path will be α_1, the same as in transmissive cells

$$\alpha_1 = -\tan^{-1}\left[\frac{\sin\beta\sin\varphi}{\cos\gamma\sin\beta\cos\varphi - \sin\gamma\cos\beta}\right]. \tag{22}$$

The variable in the return path after reflection is called α_2 and looks like

$$\alpha_2 = \tan^{-1}\left[\frac{\sin\beta\sin\varphi}{-\cos\gamma\sin\beta\cos\varphi - \sin\gamma\cos\beta}\right]. \tag{23}$$

$\mathrm{Rot2}D(\alpha)$ matrix is a function that induces a rotation. It depends on α according to the following expression:

$$\mathrm{Rot2}D(\alpha) = \begin{bmatrix} \cos\alpha & -\sin\alpha \\ \sin\alpha & \cos\alpha \end{bmatrix}. \tag{24}$$

The reflective mirror surface of the cell is represented by the mirr function.

$$\mathrm{mirr} = \begin{bmatrix} -1 & 0 \\ 0 & 1 \end{bmatrix} \tag{25}$$

$$\Delta n_1 = \sqrt{\frac{1}{\dfrac{1-[\cos\gamma\cos\beta + \sin\gamma\cos\varphi\sin\beta]^2}{n_e^2} + \dfrac{[\cos\gamma\cos\beta + \sin\gamma\cos\varphi\sin\beta]^2}{n_o^2}}} - n_o \tag{20}$$

$$\Delta n_2 = \sqrt{\frac{1}{\dfrac{1-[\cos\gamma\cos\beta - \sin\gamma\cos\varphi\sin\beta]^2}{n_e^2} + \dfrac{[\cos\gamma\cos\beta - \sin\gamma\cos\varphi\sin\beta]^2}{n_o^2}}} - n_o. \tag{21}$$

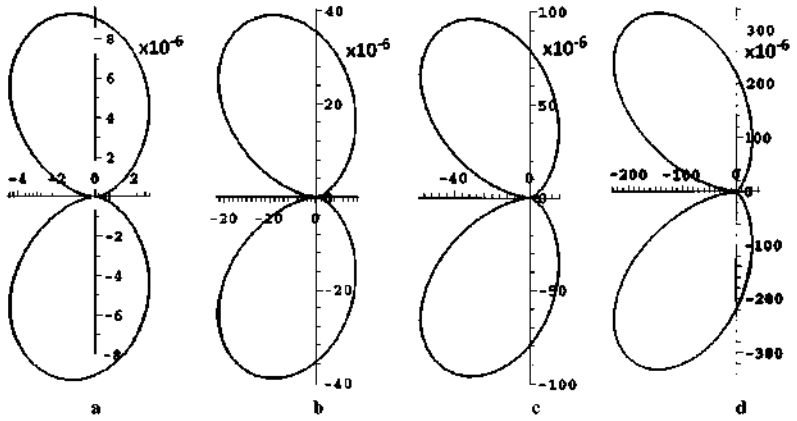

Fig. 5. Transmissive intensity for oblique incidence $\gamma = 5°$ with different pretilts: a) $\beta = 1°$, b) $\beta = 2°$, c) $\beta = 3°$, d) $\beta = 5°$. Note that scales for relative intensities are different. All axis values are normalized light intensity $\cdot 10^{-6}$.

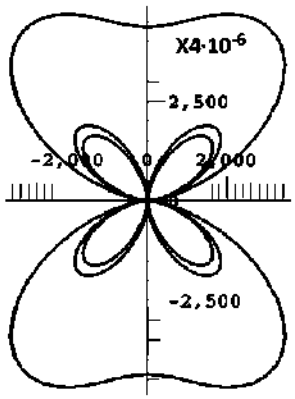

Fig. 6. Double path intensity for a pretilt $\beta = 8°$. Smaller to larger curves are normal incidence $\gamma = 0°$, $\gamma = 17°$, and $\gamma = 25°$. All axis values are normalized light intensity $4 \cdot 10^{-6}$.

The retardation induced by the birefringence of the LC material is given by the retd function that depends on both the length L, and the delay δ, of the corresponding path

$$\text{retd} = \begin{bmatrix} e^{j\left(\frac{1}{2}\delta L\right)} & 0 \\ 0 & e^{-j\left(\frac{1}{2}\delta L\right)} \end{bmatrix} \tag{26}$$

Assuming an impinging vertically polarized beam $\begin{bmatrix} 0 \\ 1 \end{bmatrix}$ at the input of a reflective cell, the output intensity is calculated from the following expression:

$$\begin{aligned} Jout =& \text{Rot2}D(-\alpha_2) \cdot \text{retd}(\delta_2) \cdot \text{Rot2}D(\alpha_2) \\ & \cdot \text{mirr} \cdot \text{Rot2}D(\alpha_1) \cdot \text{retd}(\delta_1) \cdot \text{Rot2}D(-\alpha_1) \cdot \begin{bmatrix} 0 \\ 1 \end{bmatrix}. \end{aligned} \tag{27}$$

Fig. 6 shows the intensity plots corresponding to this double path case by assigning the values specified in Table I to the variables of the $Jout$ expression. The value of the incidence angle γ is varied from 0° to 25°.

The output intensity curve starts as a four-leaf clover for a normal incident beam. The petals open up and grow as the impinging angle increases resulting in a deformed 8-shape for higher values of γ. Increasing γ further gives a much larger perfect 8-shape. The vertical and horizontal symmetries are maintained all the time due to the symmetry induced by the internal reflection. An interesting point is that the γ value for the transition of the four-leaf clover to the deformed 8-shape is closely related to the pretilt value (Fig. 7). This point will be eventually used to apply the model to the derivation of experimental data.

D. Residual Twist

Using the above described model, and the experimental setup already shown, several attempts of fitting experimental results and model predictions were carried out, probing different regions of four SXGA commercial LCOS VANs provided by Gemidis, Zwijnaarde, Belgium. However, the fitting was found to be unfeasible in most cases, for experimental data showed asymmetries that could not be corrected by optimization of the setup. Then the setup validity was checked using aluminized VAN test cells manufactured in our lab. In this case, symmetric experimental curves were obtained, and fittings were feasible. Consequently, the existence of specific features in the manufacturing process of commercial LCOS VANs resulting in variations of the LC configuration appeared to be the most realistic explanation.

These discrepancies could be explained assuming the induction of a residual twist ρ during the manufacturing process. The value of this residual twist turned out to be very small (between 1°–3°), yet it has a dramatic effect on the shape of intensity curves. The origin of this residual twist—if ultimately demonstrated—is not known. A possible explanation could come up from the intrinsic asymmetry of LCOS VAN cells. The outer plates (aluminized silicon and silica) are dissimilar. It is possible that the same surface conditioning (SiO_2 angular deposition) applied to different surfaces results in slightly different LC alignments. Anyhow, this issue deserves a more detailed study.

To include the residual twist effect in the simulation model a new function $retdrotr$ is defined incorporating the retardation and the rotation (γ and ρ)

$$retdrotr = \begin{bmatrix} e^{j\left(\frac{1}{2}\delta L\right)} & \frac{1}{2} \cdot \frac{\rho L \lambda \sin\left(\frac{\pi \Delta n L}{\lambda}\right)}{\pi \Delta n L} \\ -\frac{1}{2} \cdot \frac{\rho L \lambda \sin\left(\frac{\pi \Delta n L}{\lambda}\right)}{\pi \Delta n L} & e^{-j\left(\frac{1}{2}\delta L\right)} \end{bmatrix}. \tag{28}$$

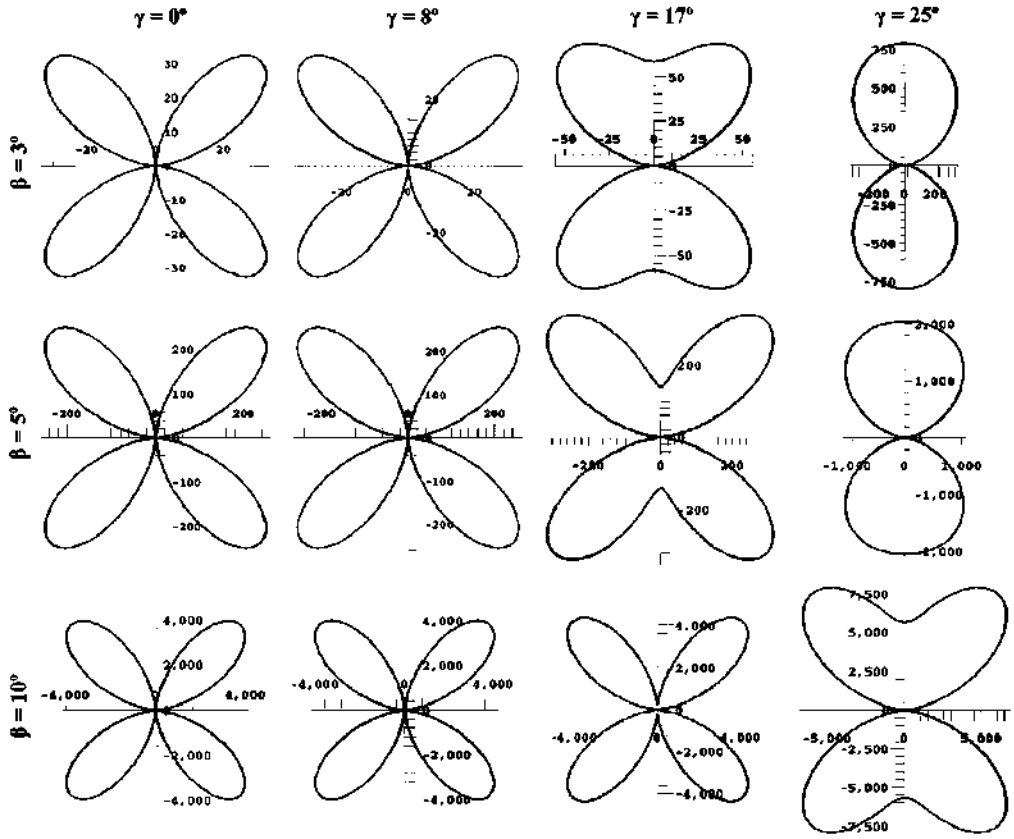

Fig. 7. Transition from four-leaf clover curve to deformed 8-shape for different pretilts. Note that relative intensity scales are different in rows and columns. All axis values are normalized light intensity $4 \cdot 10^{-6}$.

The corresponding matrix to a birefringent and optically active cell is M0 [15].

$$\mathrm{M0} = \begin{bmatrix} \cos w + j\frac{\frac{1}{2}\delta \sin w}{w} & -\frac{\rho \sin w}{w} \\ \frac{\rho \sin w}{w} & \cos w - j\frac{\frac{1}{2}\delta \sin w}{w} \end{bmatrix} \tag{29}$$

Substituting in M0 the variable w by its value $= (1/2)\sqrt{4\rho^2 + \delta^2}$, $\mathrm{M}(\rho, \delta)$ matrix is obtained, as shown in (30) at the at bottom of the page.

The output intensity obtained after the incident and reflected paths through the cell will be calculated from the following expression:

$$Jout = \mathrm{Rot2}D(-2\rho) \cdot \mathrm{Rot2}D(-\alpha_2) \cdot M(\delta_2, \rho) \cdot \mathrm{Rot2}D(\alpha_2) \cdot \mathrm{mirr} \cdot \mathrm{Rot2}D(\alpha_1) \cdot M(\delta_1, -\rho) \cdot \mathrm{Rot2}D(-\alpha_1) \cdot \begin{bmatrix} 0 \\ 1 \end{bmatrix}. \tag{31}$$

Table II shows the values employed in the following simulations, including residual twist.

The delay due to the incident path is represented by δ_1, and the delay experienced by the light in the reflected path is δ_2, as shown in (32) and (33) at the bottom of the next page.

Fig. 8 shows the curve for normal incidence as indicated in Table II. Again a four-leaf clover is obtained. Fig. 9 illustrates the cases where the incidence angle is varied from 6.5° to 25°.

From these simulated intensity curves, using the Solver Excel plug-in, the known variables (γ = angle of incidence, n_e, n_o) are fixed and the remaining (L = thickness, β = angle of pretilt, ρ = residual twist) are adjusted in the simulated curve to fit the measurements. As a reference to verify that the calculated values are correct, the same parameters are applied to the normal incidence curve.

E. Simulations and Results

Once the residual twist was included in the model, a number of simulation runs were executed (Figs. 10–12) applying different residual twists for the same set of incidence angles and

$$\mathrm{M}(\rho, \delta) = \begin{bmatrix} \cos\left(\frac{1}{2}\sqrt{4\rho^2 + \delta^2}\right) + j\frac{d \sin\left(\frac{1}{2}\sqrt{4\rho^2+\delta^2}\right)}{\sqrt{4\rho^2+\delta^2}} & -\frac{2\rho \sin\left(\frac{1}{2}\sqrt{4\rho^2+\delta^2}\right)}{\sqrt{4\rho^2+\delta^2}} \\ \frac{2\rho \sin\left(\frac{1}{2}\sqrt{4\rho^2+\delta^2}\right)}{\sqrt{4\rho^2+\delta^2}} & \cos\left(\frac{1}{2}\sqrt{4\rho^2 + \delta^2}\right) - j\frac{d \sin\left(\frac{1}{2}\sqrt{4\rho^2+\delta^2}\right)}{\sqrt{4\rho^2+\delta^2}} \end{bmatrix} \tag{30}$$

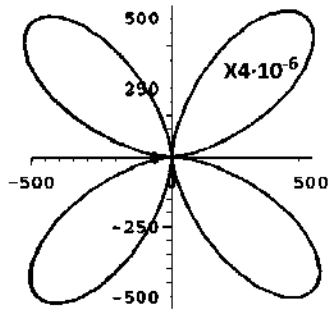

Fig. 8. Double path intensity for normal incidence including residual twist. Using the parameters indicated in Table II. All axis values are normalized light intensity $4 \cdot 10^{-6}$.

TABLE II
VALUES ADOPTED IN SIMULATIONS USING RESIDUAL TWIST

$\gamma = 0$	*original impinging beam is perpendicular to the XY plane*
$\beta = \frac{3\pi}{180}$	*radians corresponding to 3° pretilt angle*
$\rho = \frac{\pi}{180}$	*radians corresponding to 1° residual twist*
$n_e = 1.65$	*extraordinary index*
$n_o = 1.5$	*ordinary index*
$L = 1.6$	*cell thickness in μm*
$\lambda = 543$	*wavelength in nm*
$bk = 2{\cdot}10^{-6}$	*normalized background intensity of incident light*

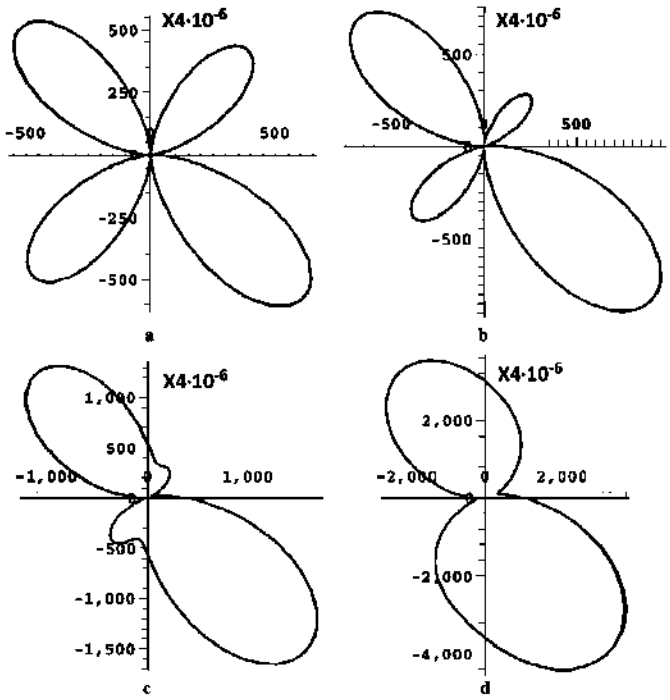

Fig. 9. Double path intensity for oblique incidence including residual twist. (a) $\gamma = 6.25°$. (b) $\gamma = 12.5°$. (c) $\gamma = 18.75°$. (d) $\gamma = 25°$. Note that scales are different. All axis values are normalized light intensity $4 \cdot 10^{-6}$.

pretilts. As seen in the figures, even a residual twist as small as $\rho = 1°$ introduces remarkable asymmetry on the otherwise symmetric transmission curves. This fact makes feasible the fitting of asymmetric experimental data to the transmission predicted by the model, thus allowing the calculation of relevant parameters.

IV. EXPERIMENTAL VALIDATION

As mentioned above, the model has been tested for validation using experimental measurements. The procedure was as follows. First a set of about 5000 points were recorded while the cell performed a full rotation about the Z axis. The acquisition was averaged for several rotations and the background signal was subtracted. Then data were averaged angularly by gathering groups of 6–8 contiguous points of raw data and assigning the average to the central angle. Two data sets were acquired simultaneously on every experiment, one corresponding to a selected oblique incidence and the other to normal incidence.

A nonlinear least-squares fitting of oblique data, using Solver, was performed. The adjusted variables were cell thickness, pretilt and residual twist angle. Once convergence was achieved, the found values were substituted in the model expression for normal incidence and the predicted transmission was compared to actual experimental data without performing any correction. The fit is accepted if a good agreement is obtained for both curves with the same values.

Fig. 13 is an example of experimental validation. An LCOS VAN commercial cell ($n_e = 1.5595$, $n_o = 1.4775$) was measured with a laser wavelength $\lambda = 543$ nm, and an incidence angle $\gamma = 7.51°$ (Fig. 13, top). The normal incidence curve (Fig. 13, bottom) was acquired at the same time. The oblique data showed a noticeable asymmetry that marred any attempt of fitting unless residual twist is considered. Convergence of the

$$\delta_1 = \frac{2L\left[\sqrt{\frac{1}{\frac{1-(\sin\gamma\cos\varphi\sin\beta+\cos\gamma\cos\beta)^2}{n_e^2}+\frac{(\sin\gamma\cos\varphi\sin\beta+\cos\gamma\cos\beta)^2}{n_o^2}}}-n_o\right]\cdot\pi}{\lambda\cos\gamma} \tag{32}$$

$$\delta_2 = \frac{2L\left[\sqrt{\frac{1}{\frac{1-(\sin\gamma\cos\varphi\sin\beta+\cos\gamma\cos\beta)^2}{n_e^2}+\frac{(-\sin\gamma\cos\varphi\sin\beta+\cos\gamma\cos\beta)^2}{n_o^2}}}-n_o\right]\cdot\pi}{\lambda\cos\gamma}. \tag{33}$$

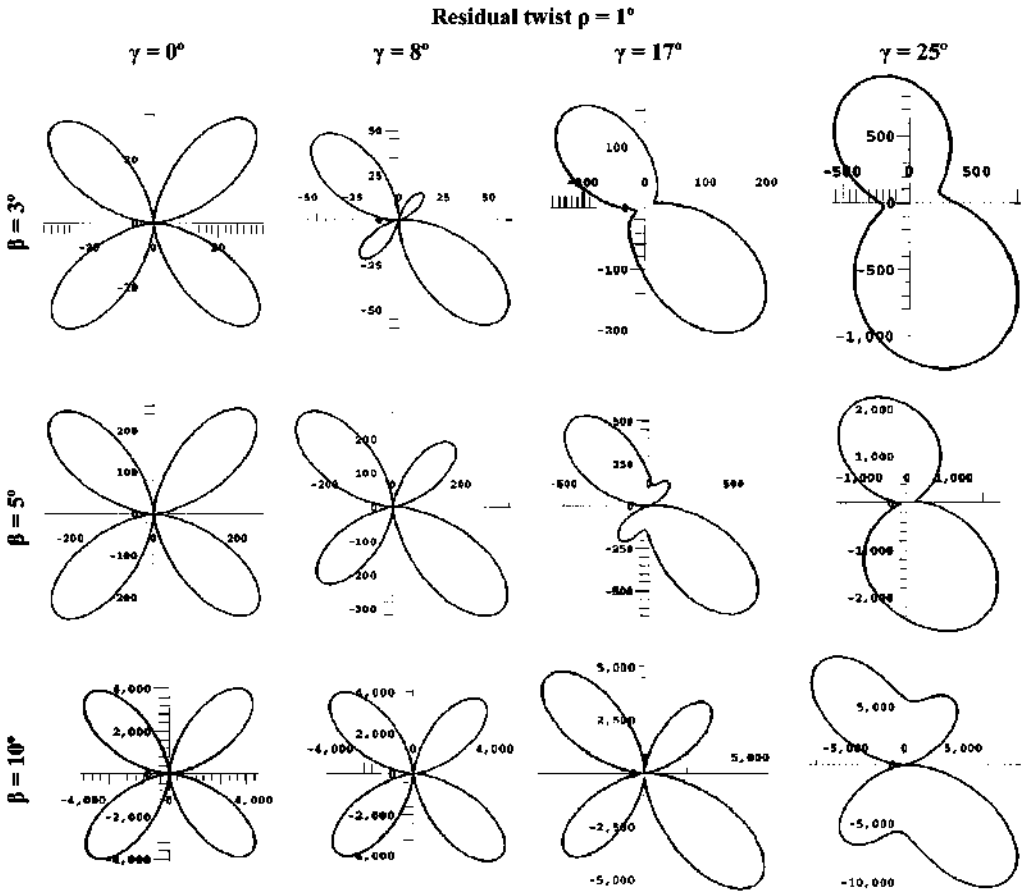

Fig. 10. Effect of residual twist on trasmission curves for different incidence angle and pretilts (I). All axis values are normalized light intensity $4 \cdot 10^{-6}$.

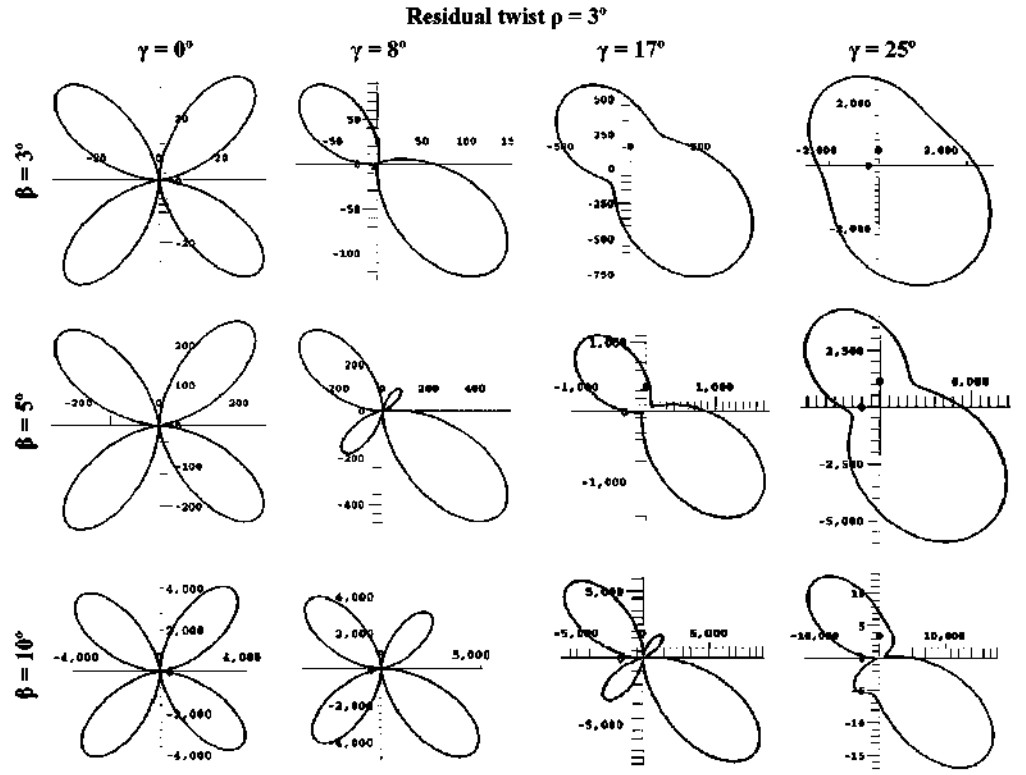

Fig. 11. Effect of residual twist on trasmission curves for different incidence angle and pretilts (II). All axis values are normalized light intensity $4 \cdot 10^{-6}$.

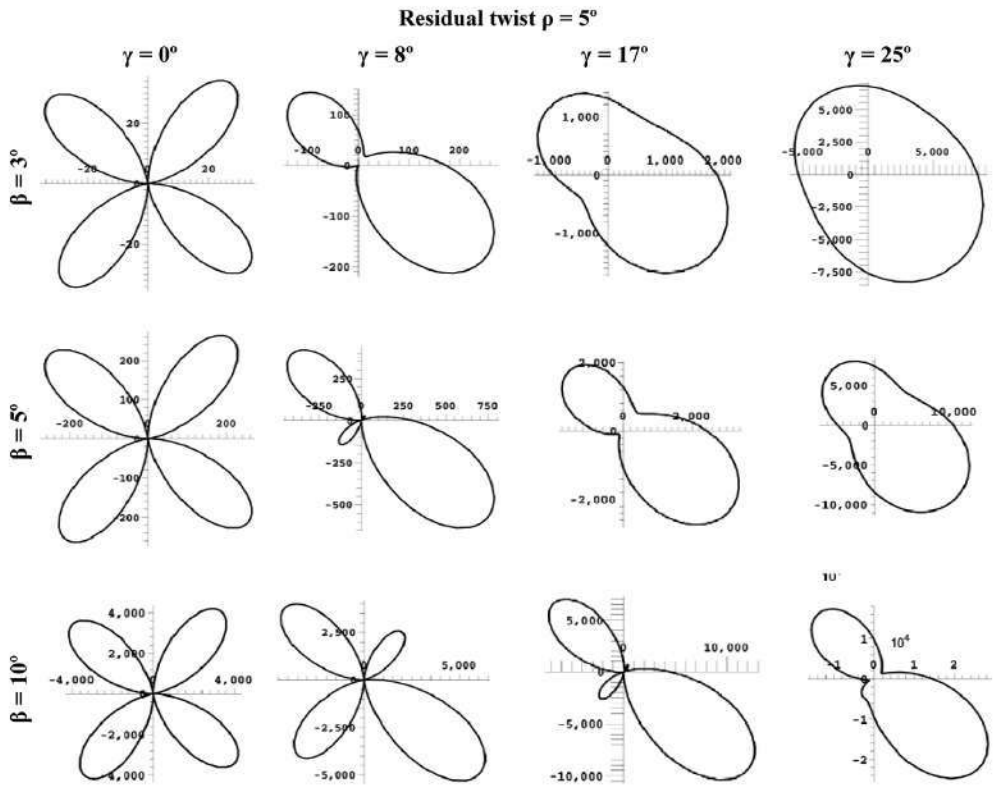

Fig. 12. Effect of residual twist on trasmission curves for different incidence angle and pretilt (III). All axis values are normalized light intensity $4 \cdot 10^{-6}$.

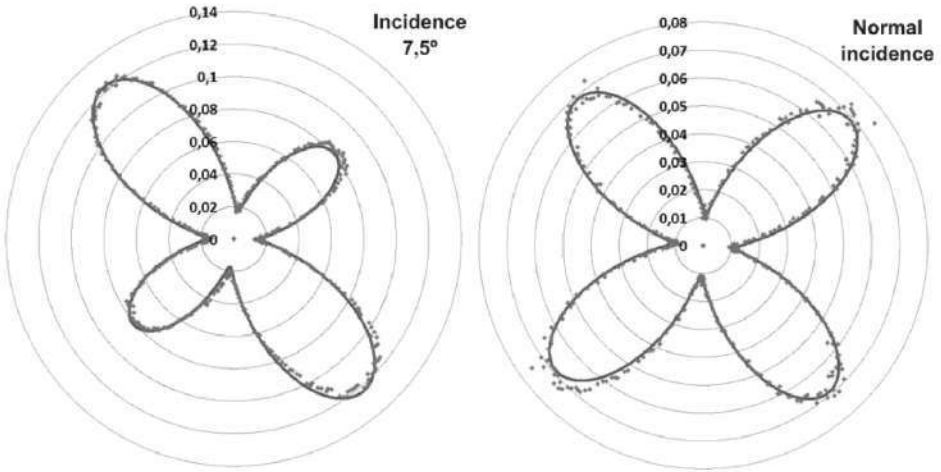

Fig. 13. Validation of the model with experimental data. ($n_e = 1.5595$, $n_o = 1.4775$, and $\lambda = 543$ nm).

nonlinear least-squares fit of oblique data, gave the following set of parameters:

$$\textbf{Thickness} = \mathbf{2.4}\ \mu\text{m} \qquad \textbf{Pretilt} = \mathbf{2.84}^\circ$$
$$\textbf{Residual twist} = \mathbf{2.26}^\circ$$

The same values were used to plot the normal incidence curve (bottom) superimposed to the experimental data. As seen in the figures, a good matching between calculated and experimental data is achieved in both cases.

If required, the above model could be extended to variable pretilt or residual twist throughout the cell. This would require splitting the LC layer into as many slices as required for the model to accurately describe the tilt or twist profile.

V. Conclusion

A conceptually simple optical procedure for variable separation in LCOS VAN displays has been demonstrated. The procedure allows accurate measurements beyond tolerances of relevant parameters such as sample thickness and induced pretilt. An independent parameter, assigned to a residual twist, has proved to be necessary to account for asymmetries in experimental transmission curves. Data validation is achieved by comparing data for normal or different oblique incidences with their corresponding model plots, employing the same adjusted parameters in all cases.

REFERENCES

[1] R. Lu, Q. Hong, S.-T. Wu, K.-H. Peng, and H.-S. Hsieh, "Quantitative comparison of color performances between IPS and MVA LCDs," *J. Display Technol.*, vol. 2, no. 4, pp. 319–326, Dec. 2006.

[2] X. J. Yu and H. S. Kwok, "Fast response film-compensated liquid crystal on silicon display," *Appl. Phys. Lett.*, vol. 89, p. 031104, 2006.

[3] N. Xiangyi, X. Haiqing, L. Ruibo, W. Thomas X., and W. Shin-Tson, "Pretilt angle effects on liquid crystal response time," *J. Display Technol.*, vol. 2, no. 3, pp. 280–283, Sep. 2007.

[4] S. T. Tang and H. S. Kwok, "Transmissive liquid crystal cell parameters measurement by spectroscopic ellipsometry," *J. Appl. Phys.*, vol. 89, pp. 80–85, 2001.

[5] K. Y. Han, T. Miyashita, and T. Uchida, "Accurate measurement of pretilt angle in the liquid crystal cell by an improved crystal rotation method," *Mol. Cryst. Liq. Cryst.*, vol. 241, pp. 147–157, 1994.

[6] J. S. Gwag, S. H. Lee, K. Park, W. S. Park, K. Han, and C. G. Jhun, "Simple method for measuring the high pretilt angle of nematic liquid crystals," *J. Appl. Phys.*, vol. 8, p. 4936, 2003.

[7] B. G. Rho, J. S. Kim, and J. K. Kim, "Simultaneous measurement of pretilt angle and cell gap of LC cells by using an improved crystal rotation method," in *Proc. Asia Display*, 1998, vol. 98, pp. 245–248.

[8] M. Kawamura, Y. Goto, and S. Sato *et al.*, "Novel real-time measurement of cell parameters in reflective liquid crystal cells by using a circularly homogeneously aligned liquid crystal cell," in *Proc. SPIE'03*, 2003, vol. 5213, pp. 250–257.

[9] D. Cuypers, H. De Smet, G. Van Doorselaer, J. Van Den Steen, and A. Van Calster, "Measurement methodology for vertically aligned nematic reflective displays," in *Proc. SPIE'03*, 2003, vol. 5002, p. 62.

[10] J. Li, C. Wen, S. Gauza, R. Lu , and S. Wu, "Refractive indices of liquid crystals for display applications," *J. Display. Technol.*, vol. 1, no. 1, pp. 51–61, Sep. 2005.

[11] S. J. Hwang, S.-T. Lin, and C.-H. Lai, "A novel method to measure the cell gap and pretilt angle of a reflective liquid crystal display," *Opt. Commun.*, vol. 260, pp. 614–620, 2006.

[12] J. S. Hsu, B. J. Liang, and S. H. Chen, "A simple method for determining the pretilt angle of a vertically aligned reflective LCD," *IEEE Trans Electron. Devices*, vol. 52, no. 5, pp. 918–921, May 2005.

[13] B. Cerrolaza, M. A. Geday, J. M. Otón, X. Quintana, and N. Bennis, "Measuring thickness and pretilt in reflective vertically aligned nematic liquid crystal displays," *Mol. Cryst. Liq. Cryst.*, vol. 494, pp. 222–230, 2008.

[14] R. Clark Jones, "A new calculus for the treatment of optical systems," *J. Opt. Soc. Amer.*, vol. 31, pp. 488–493, 1941.

[15] M. A. Geday and A. M. Glazer, "A new view of conoscopic illumination of optically active crystals," *J. Appl. Cryst*, vol. 35, no. 2, pp. 185–190, 2002.

Beatriz Cerrolaza received the M.S. degree from the Universidad Públlica de Navarra (UPNA), Spain, in 2006, and where she is currently working toward the Ph.D. degree in telecommunication engineering.

In 2008, she was visiting researcher for four months with TFCG Microsystems, IMEC, Ghent, Belgium. Her main research activities during the stay consisted in the study of Motion Blur and measurement techniques of MPRT parameter.

Morten Andreas Geday received the integrated B.S. and M.S. degrees in chemistry and biotechnology from Aarhus Universitet, Denmark, in 1997, and the Doctoral degree in condensed matter physics from Jesus College, University of Oxford, Oxford, U.K., in 2001.

He spent three years as project responsible at Oxford Cryosystems Ltd, U.K. Since 2004 he has been working at the Polytechnical University of Madrid, Madrid, Spain, as research fellow and research professor. His principal research interest is liquid crystal-device development and modelling, both for display and light modulation.

Xabier Quintana received the M.S. degree in telecommunication engineering in 1990, and the Ph.D. degree from the Polytechnic University of Madrid, Spain, in 1993.

Since 1993, his research area has been focused on liquid crystal microdisplays, ferroelectric and antiferroelectric materials and more recently on liquid crystal devices for non display photonic applications. He is currently is Associate Professor at the Polytechnic University of Madrid, Spain. He has co-authored over 50 international publications and presented more than 100 communications in international conferences and symposia in this area.

José Manuel Otón is Full Professor at the Department of Photonic Technology in the Polytechnic University of Madrid, Spain. He is involved in research on liquid crystal devices and applications for more than 25 years. During this time he has carried out over 30 research projects, of which 10 are European R&D joint projects on liquid crystal microdisplays, ferroelectric and antiferroelectric devices and non-display photonic applications. He has co-authored over 120 international publications and presented more than 250 communications in international conferences and symposia in this area.